Mixing and Transport in Coastal River Plumes

Alexander R. Horner-Devine,[1] Robert D. Hetland,[2] and Daniel G. MacDonald[3]

[1]Department of Civil and Environmental Engineering, University of Washington, Seattle, Washington 98195; email: arhd@uw.edu

[2]Department of Oceanography, Texas A&M University, College Station, Texas 77843

[3]Department of Civil and Environmental Engineering, University of Massachusetts Dartmouth, Dartmouth, Massachusetts 02747

Annu. Rev. Fluid Mech. 2015. 47:569–94

First published online as a Review in Advance on October 1, 2014

The *Annual Review of Fluid Mechanics* is online at fluid.annualreviews.org

This article's doi: 10.1146/annurev-fluid-010313-141408

Keywords

coastal ocean circulation, stratified flows, turbulence, geophysical flows

Abstract

River plumes are generated by the flow of buoyant river water into the coastal ocean, where they significantly influence water properties and circulation. They comprise dynamically distinct regions spanning a large range of spatial and temporal scales, each contributing to the dilution and transport of freshwater as it is carried away from the source. River plume structure varies greatly among different plume systems, depending on the forcing and geometry of each system. Individual systems may also exhibit markedly different characteristics under varied forcing conditions. Research over the past decade, including a series of major observational efforts, has significantly improved our understanding of the dynamics and mixing processes in these regions. Although these studies have clarified many individual processes, a holistic description of the interaction and relative importance of different mixing and transport processes in river plumes has not yet been realized.

1. INTRODUCTION

Rivers carry more than one-third of land-based precipitation to the ocean (Trenberth et al. 2007), focusing large freshwater fluxes through narrow outlets along the coast (Milliman & Farnsworth 2011). For example, the Mississippi River drains approximately 40% of the continental United States to two distributaries, each of which is less than 1 km wide (Milliman & Meade 1983). The impact of the terrigenous material carried by the river water into these ecologically sensitive coastal waters depends strongly on the physical processes that transport and transform the buoyant freshwater in the region around the river mouth as it merges with deeper, salty ocean waters. In particular, the dilution rates and along-coast transport rates of the river-borne material are determined by a suite of processes, including stratified-shear mixing, frontal processes, geostrophic transport, and wind forcing. In the coastal ocean, these discharges form river plumes, which are distinct regions where water properties and dynamics are significantly influenced by the riverine freshwater. River plumes are also sometimes referred to as regions of freshwater influence (ROFIs), although this term is more commonly reserved for systems with multiple freshwater sources or shallow frictional shelves. The distinguishing dynamical feature of a river plume is the horizontal advection of freshwater from the river mouth that defines the shape and character of the plume.

River plumes are fundamentally multiscale flow structures, which occur in a range of sizes and shapes. The primary independent parameters that determine the structure and scale of individual plumes are freshwater discharge, tidal amplitude, coastline bathymetry/geometry, ambient ocean currents and water properties, wind stress, and Earth's rotation. Of these parameters, freshwater discharge typically has the most variability within a system, often changing over an order of magnitude within a single system, and among different systems, varying by over four orders of magnitude. This large variability results in significant structural and dynamical differences among systems. For example, the River Teign has a small discharge (5 $m^3\ s^{-1}$) and forms a buoyant layer a few meters thick seaward of the estuary mouth after each ebb tide (Pritchard & Huntley 2006); this plume dissipates in a matter of hours and forms anew with each tide. The Merrimack River plume is of moderate size (300 $m^3\ s^{-1}$) and occasionally persists between tides, depending on the wind (MacDonald et al. 2007). The Columbia River plume is large (10,000 $m^3\ s^{-1}$), and it is strongly affected by the tide near the estuary mouth but is persistent and governed by other processes far beyond this tidal region (Horner-Devine et al. 2009, Hickey et al. 2010). The Mississippi River plume is very large (30,000 $m^3\ s^{-1}$) and is in a region with very small tides (Wright & Coleman 1971). It forms a huge, persistent plume that dominates the coastal circulation along most of the Louisiana and Texas shelves (Cochrane & Kelly 1986, Murray 1998, Zhang & Hetland 2012, Zhang et al. 2012).

The impact of a plume on shelf circulation and ecosystem health depends on the dilution rate and transport processes within the plume. Dilution is controlled primarily by vertical mixing, which increases the salinity of the plume and decreases the concentration of river-borne materials. Transport in the plume is controlled primarily by horizontal advection, which is driven in large part by plume buoyancy, and thus by mixing. Here, we focus specifically on the processes that contribute to mixing (Section 3) and transport (Section 4) in river plumes. Most analyses and observations consider processes active in specific regions of the plume in isolation. We begin, therefore, by introducing the basic dynamical regions of the plume. The objective of this article is not to provide a comprehensive review of previous research on river plumes (see O'Donnell 2010, Chant 2011, Hetland & Hsu 2013) but rather to discuss and synthesize the processes relating to mixing and transport to gain a more holistic picture of how the different processes acting at a wide range of spatial and temporal scales interact.

2. THE DYNAMICAL REGIONS OF RIVER PLUMES

The dominant dynamical balance differs significantly among each region of a river plume, motivating a description of the river plume structure in terms of four dynamical regions (Garvine 1984, Hetland 2005, Horner-Devine et al. 2009).

First, in the source region, the buoyancy and momentum that initiate a river plume are determined by estuarine processes, which are responsible for the initial transformation of river discharge. Nash et al. (2009) show that the median salinity, thickness, and turbulent mixing rates of the near-field Columbia River plume are set by the competition between the stratifying influence of river discharge and the mixing provided by tidal energy within the estuary, as expressed by the estuarine Richardson number,

$$\mathrm{Ri}_E = g'_f \frac{Q_f}{W_E\, u^3_{\mathrm{tidal}}}. \quad (1)$$

The reduced gravity is defined in general as $g' = g(\Delta\rho/\rho_o)$, where g is the gravitational acceleration, and $\Delta\rho$ is the density difference relative to background ocean water ρ_o. Here g'_f represents the density difference between fresh river water and salty ocean water, Q_f is the river discharge, W_E is the estuary width, and u_{tidal} is the tidal velocity. More information on estuaries is presented in recent reviews by MacCready & Geyer (2010) and Geyer & MacCready (2014).

In strongly forced systems, the estuarine discharge separates from the bottom near the river mouth and forms the buoyant layer (**Figure 1**). The liftoff point is the location of the bottom-attached salt front where the upper layer loses contact with the bottom and the upper-layer Froude number $\mathrm{Fr}_1 = 1$. Here, $\mathrm{Fr}_1 = u(g'h)^{-1/2}$, and u and h are the upper-layer velocity and depth, respectively. The dynamics of the liftoff process are explained by inviscid two-layer hydraulic theory and are analogous to the case of strong barotropic forcing (Armi & Farmer 1986, Farmer & Armi 1986), in which the point of hydraulic control ($\mathrm{Fr}_1 = 1$) is forced seaward from the point of the smallest plume cross section and flow in the lower layer is arrested. Internal hydraulic theory predicts that liftoff may result from either a deepening (Farmer & Armi 1986) or widening (Armi & Farmer 1986) of the flow. In the deepening case, the interface remains horizontal seaward of the liftoff point, whereas it shoals when the flow widens. Liftoff is often observed at or near a sill, where depths are beginning to increase; however, shoaling of the surface layer is consistently observed, indicative of the importance of lateral flow expansion. Finally, the liftoff front may be maintained at an angle to the oncoming flow such that local Froude numbers are substantially supercritical (MacDonald & Geyer 2005). In these cases, the liftoff front must be anchored at a position in the channel where local Froude numbers are critical, with the remainder of the front defined by a Froude angle $\psi = \sin^{-1}\mathrm{Fr}_1^{-1}$, such that Fr_1 is critical with respect to flow normal to the front.

Second, the jet-like near-field region begins at liftoff, or at the river mouth if liftoff occurs in the estuary, and is generally considered to be the region where the river momentum exceeds the buoyancy of the plume layer (i.e., $\mathrm{Fr}_1 > 1$). Thus, the near-field region is generally considered to end where the flow ceases to be supercritical ($\mathrm{Fr}_1 = 1$; Hetland 2005, 2010), although this point can be difficult to identify because Fr_1 gradually transitions from supercritical to subcritical over a significant fraction of the near-field area. The near field has much in common with an engineering jet (e.g., Jirka et al. 1981, Jones et al. 2007), although its large aspect ratio isolates it from significant lateral mixing (Chen & MacDonald 2006).

The near-field momentum balance is dominated by barotropic and baroclinic pressure gradients, turbulent interfacial stress between the discharging plume layer and the underlying ambient water, and flow acceleration (McCabe et al. 2009), with the interfacial stress as the primary driver of plume deceleration under low discharge conditions and peak ebb tide (Kilcher et al. 2012). In

Source region: the estuarine region, inside the river mouth, where the initial buoyancy and momentum of the river plume are set

Liftoff: the location of the bottom attached salt front, where the buoyant outflow loses contact with the bottom

Fronts: sharp lateral gradients in fluid density that form internally and, most commonly, on the boundaries of the plume

Near-field region: the jet-like region of initial plume expansion where the momentum of the plume layer dominates over its buoyancy, resulting in intense mixing

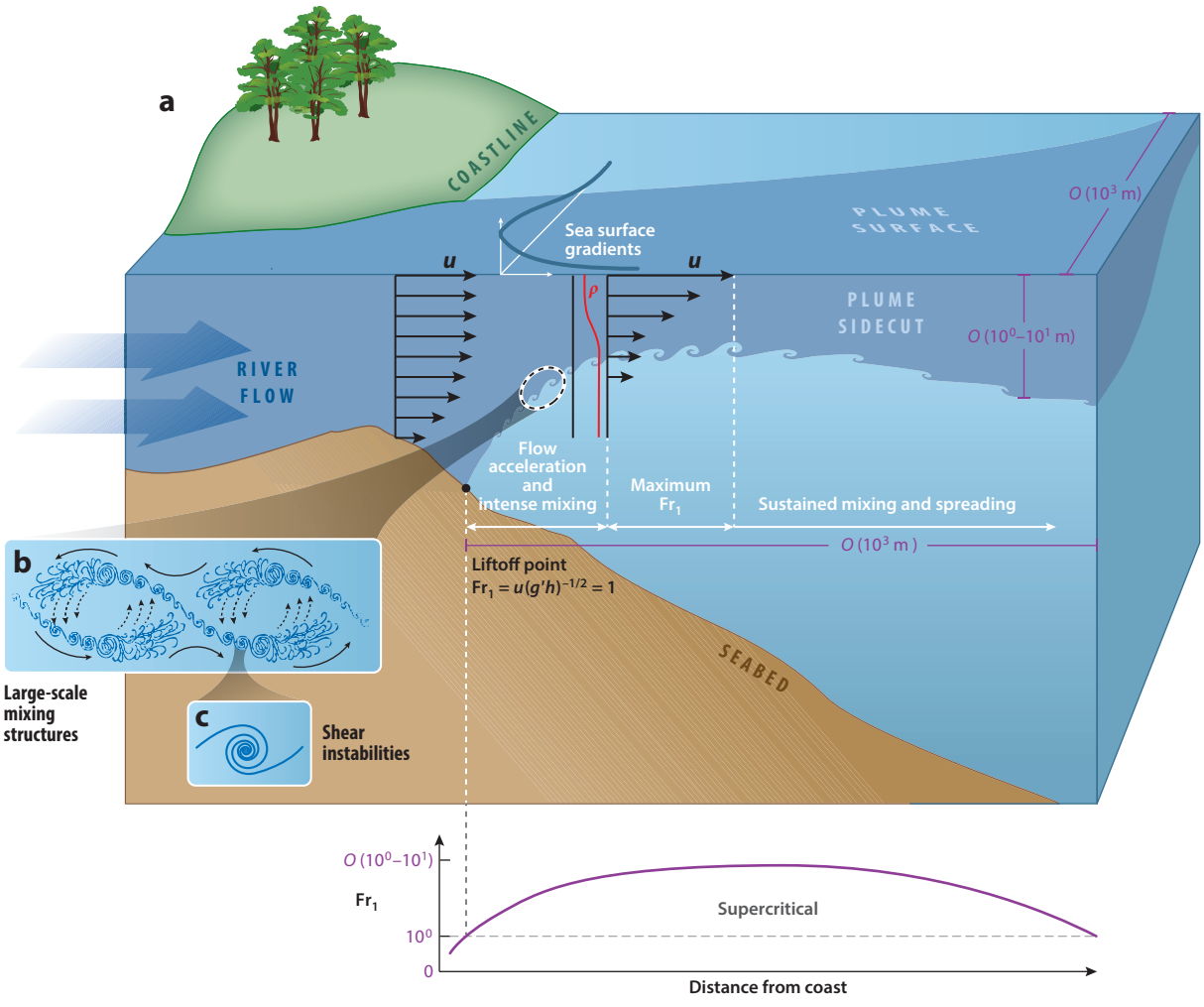

Figure 1

(*a*) Schematic representation of the plume liftoff process and the near-field plume region. (*b*) Large-scale mixing structures in the flow acceleration region. Panel *b* adapted from Geyer et al. (2010). (*c*) Shear instabilities comprising the large-scale mixing structures.

cases in which the river mouth is wide compared to the Rossby radius, $L_R = (gh)^{1/2}/f$, a near-field region will not exist, and the discharge will exit the estuary as a far-field plume, attached to the right bank (in the Northern Hemisphere). In regions with large tides, the dynamics in the near-field region are strongly time dependent, and the near-field plume is also referred to as the tidal plume (Horner-Devine et al. 2009, Kilcher & Nash 2010, Kilcher et al. 2012).

Mid-field region: the region where Earth's rotation begins to dominate, arresting plume spreading and turning the plume in the downcoast direction

Third, the mid-field is the region where inflowing river water transitions from the inertial near-field jet into a geostrophic or wind-dominated far-field plume. Lateral spreading is arrested, inflow momentum is lost, and plume dynamics are increasingly dominated by Earth's rotation. In most systems, the plume is initially directed offshore and turns in the mid-field region to form a shore-parallel coastal current. This process is driven by Earth's rotation and is associated with a corresponding increase in centripetal acceleration (Garvine 1987, McCabe et al. 2009), although

ambient alongshore currents may also contribute to turning the plume (Fong & Geyer 2002). Under sufficiently low wind conditions, some outflows can form a recirculating bulge region in the mid-field, as discussed in Section 4.3. The momentum balance in the mid-field is dominated by the Coriolis force, centripetal acceleration, and the cross-stream internal pressure gradient (Garvine 1987, Yankovsky & Chapman 1997, Horner-Devine 2009, McCabe et al. 2009).

Finally, the far field is the region beyond the mid-field in which the plume no longer has a memory of the initial momentum of the river discharge, and the dynamics are primarily governed by Earth's rotation, buoyancy, wind stress, and sometimes bottom stress. This region may extend hundreds of kilometers from the mouth. When winds and ambient currents are not sufficient to force the plume offshore, the far-field plume forms a geostrophic coastal current that transports diluted river water in the direction of Kelvin wave propagation (hereafter referred to as downcoast). The structure, dynamics, and propagation speed of the coastal current depend on the shelf slope (Avicola & Huq 2002, Lentz & Helfrich 2002) and whether the plume is in contact with the bottom (Yankovsky & Chapman 1997).

The anatomy of the prototypical large-scale plume, which is composed of all these regions, is presented schematically in **Figure 2**. Numerical and laboratory model studies with simplified geometry generate plumes similar to the prototypical plume (e.g., Fong & Geyer 2002, Avicola & Huq 2003a, Horner-Devine et al. 2006), and field observations from a number of large-scale plume systems indicate that they have a similar structure during low-wind conditions (e.g., Chant et al. 2008, Hickey et al. 2010). However, it important to note that some of these regions will be absent in many plumes, and thus the structure of the plume may be quite different than the prototypical plume. This variability in plume structure and behavior is discussed in Section 5.

Bulge: an unsteady, anticyclonic eddy circulation that can form offshore of the river mouth under certain conditions, expand continuously, and accumulate a fraction of the river discharge

Far-field region: the region beyond the mid-field where the plume water has lost all memory of the inflow momentum but is still distinct from the ambient receiving water

3. MIXING

3.1. Local Mixing: Regions and Processes Within the Plume

Mixing in river plumes may be defined as the transport of buoyancy and momentum across isopycnal surfaces (e.g., Sherman et al. 1978, Ivey et al. 2008, Stacey et al. 2011). Because of the very

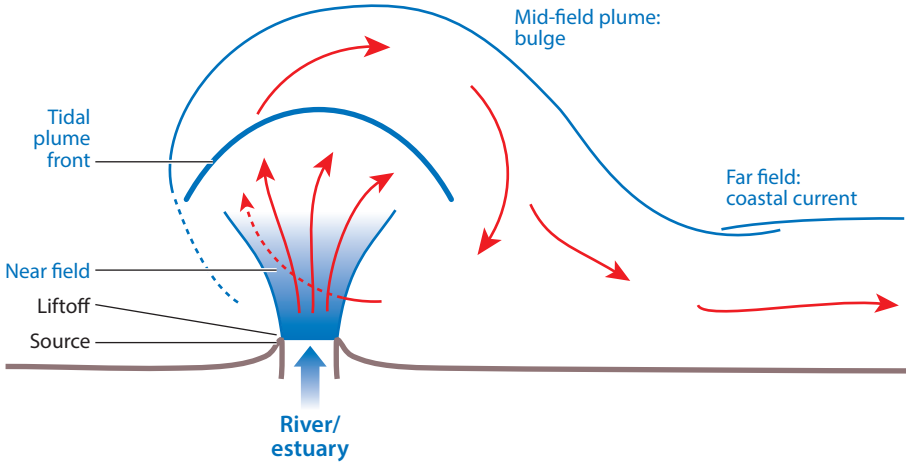

Figure 2

Schematic representation of the prototypical plume comprising all dynamical regions. Other plume morphologies are discussed in Section 5 and shown in **Figure 5**.

small aspect ratio of most river plumes, $\mathcal{O}(10^{-3})$, the vertical turbulent flux of density, $\overline{w'\rho'}$, is generally considered to be dominant over the horizontal turbulent fluxes.

In practice, the intensity of turbulence is often quantified based on the turbulent kinetic energy dissipation rate ϵ, which can be estimated from field measurements using microstructure techniques (e.g., Moum et al. 1995) or overturn scales (Orton & Jay 2005). Turbulent mixing is typically quantified in terms of the turbulent vertical salt flux $\overline{w'S'}$ or the buoyancy flux $B = (g/\rho)\overline{w'\rho'}$. The buoyancy flux in river plumes has been estimated directly using control volume techniques (MacDonald & Geyer 2004, McCabe et al. 2008) or dye releases (Houghton et al. 2004, 2009). In energetic mixing regions, the plume maintains a gradient Richardson number, Ri_g, of order 0.25, and an order unity turbulent Froude number, Fr_t, resulting in maximal mixing efficiencies $\Gamma \simeq 0.2$ (e.g., Ivey & Imberger 1991) and allowing buoyancy flux to be estimated from dissipation measurements as $B = \Gamma\epsilon$. Here, the gradient Richardson and turbulent Froude numbers are defined according to $\mathrm{Ri}_g \equiv N^2(\partial_z u)^{-2}$, where $N^2 = -g\partial_z u\rho_0^{-1}$, and $\mathrm{Fr}_t = u_{\mathrm{rms}}N^{-1}L^{-1}$, where L is the scale of the large eddies.

The net impact of mixing in a specific region of the plume depends not only on the intensity of the turbulence and the density gradient available for mixing, but also on the spatial extent of the active mixing area and the duration of the mixing event. Mixing throughout the plume can be related to the discharge by considering the plume in isohaline coordinates, as described by Hetland (2005). The volume of plume water contained within an isohaline, with salinity S_A, can be related to the discharge and the average mixing across that isohaline surface as

$$S_A \frac{\partial}{\partial t} V_{fA} = S_A Q_f + \int_{S_A} \overline{w'S'}\, dA, \tag{2}$$

where V_{fA} is the volume of freshwater contained within the isohaline S_A, and $\overline{w'S'}$ is the vertical salt flux across the isohaline surface. In the limit of no mixing, $\overline{w'S'} = 0$, the plume expands like a balloon. In the steady-state limit, the input of freshwater is balanced by mixing across the isohaline surface. Hetland (2005) continues this analysis by differentiating Equation 2 with respect to salinity so that mixing and discharge can be related in specific regions of the plume, as defined by particular salinity ranges. Typically, lower salinity classes of the plume near the source are associated with stronger mixing and are smaller; higher salinity classes have weaker mixing and are larger.

3.1.1. Mixing in the near-field region. Some of the most intense turbulence and mixing in the plume occur in the near-field region, where ϵ values are observed to be as high as 10^{-4} to 10^{-3} m^2 s^{-3} (MacDonald & Geyer 2004, MacDonald et al. 2007, McCabe et al. 2008, Kilcher et al. 2012). As described in Section 2, plume expansion seaward of the liftoff point ($\mathrm{Fr}_1 = 1$) causes the plume interface to shoal rapidly, following internal hydraulic theory (Armi & Farmer 1986). Shoaling of the interface in turn causes the upper layer to accelerate according to the inviscid upper-layer momentum equation, $u\,\partial_x u = -g'\,\partial_x h$, where h is the interface depth. Acceleration in the upper layer and shoaling isopycnals increase Fr_1 and drive local Ri_g values down, resulting in intense mixing. Turbulence is most intense in the shoaling region immediately seaward of the liftoff point and subsequently decreases throughout the near field (Luketina & Imberger 1987, MacDonald et al. 2007, McCabe et al. 2008).

The decrease in mixing is a consequence of the entrainment of low-momentum, salty ambient water into the plume, which will decelerate the plume and decrease the Froude number according to

$$\frac{\partial \mathrm{Fr}_1}{\partial x} = \frac{\frac{\partial W}{\partial x} hu(\mathrm{Fr}^2 + 2) - 3w_e W \mathrm{Fr}^2}{2Wh\mathrm{Fr}(\mathrm{Fr}^2 - 1)}, \tag{3}$$

where W is the plume width, w_e is an entrainment velocity of ambient fluid across the base of the plume, and x is in the streamwise direction (Hetland 2010). Thus, the seaward evolution of Fr_1 results from competition between the acceleration associated with spreading and the deceleration associated with mixing, the left and right terms in the numerator, respectively.

Plume spreading enhances mixing in the near-field region by increasing shear as described above and also by increasing the planform area over which mixing occurs (Yuan & Horner-Devine 2013). The expansion is driven by lateral density gradients and the resulting stream-normal barotropic pressure gradient, which is particularly strong in the immediate vicinity of the river mouth, as discussed by McCabe et al. (2009). The lateral fronts expand away from the axis of the plume as freely propagating gravity current fronts, resulting in a spreading rate that is proportional to the local internal gravity wave speed, $c = (g'h)^{1/2}$ (Wright & Coleman 1971, Hetland & MacDonald 2008, Chen et al. 2009, Hetland 2010, Yuan & Horner-Devine 2013). In addition to these mechanisms, recent observations by MacDonald & Chen (2012) provide evidence that spreading may locally enhance turbulence as the divergence of the plume stretches the turbulent eddies. This effect was not observed in subsequent laboratory experiments of spreading plumes (Yuan & Horner-Devine 2013), however, and the impact of spreading on local turbulent mixing processes remains uncertain. McCabe et al. (2009) discuss the relative role of rotation in plume spreading. They argue that the important quantity for plume spreading is the sum of the stream-normal pressure gradient and the Coriolis term. Spreading will vary across the plume; the pressure and Coriolis terms are in opposition on the upcoast edge of the plume but are in concert on the downcoast edge.

Mixing in river plumes is dominated by stratified-shear flow instabilities (Stacey et al. 2011, Yuan & Horner-Devine 2013), particularly Kelvin-Helmholtz (KH) instabilities (Thorpe 1969, Kantha et al. 1977, Trowbridge 1992, Smyth & Moum 2000). In the near-field plume, strong shear, on the order of 0.5–1 s^{-1}, is often present at the plume base, with density differences of 15–20 kg m^{-3} between the plume and ambient waters. Corresponding gradient Richardson numbers are maintained at approximately 0.25, providing sufficient conditions for the development of KH billows (e.g., Thorpe 1973, Smyth et al. 2001) and subsequent turbulent mixing. KH-like structures have been observed acoustically in estuarine and plume flows (Tedford et al. 2009, Geyer et al. 2010) at larger scales, although Geyer et al. (2010) indicate that these are self-similar structures at scales an order of magnitude larger than the KH billows actually responsible for mixing (**Figure 1*b***). The size of KH billows is set by the Ozmidov scale, $L_o = \varepsilon^{1/2} N^{-3/2}$, which is $\mathcal{O}$(10 cm) in strongly stratified plume regions. Less than 10% of the interfacial volume is occupied by coherent overturn structures capable of initiating significant mixing (MacDonald et al. 2013). Turbulent dissipation rates and turbulent buoyancy fluxes resulting from stratified-shear mixing processes are best nondimensionalized by the quantity $g'\Delta U$ (Imberger & Ivey 1991, MacDonald & Geyer 2004).

3.1.2. Wind and wave mixing. Wind stress generally results in lower turbulence levels than are observed in more energetic areas such as the near field or plume front. Houghton et al. (2009) use dye release measurements in the far-field plume and show that the salt fluxes vary from approximately 5×10^{-5} kg m s^{-1} during low wind conditions to 3×10^{-4} kg m s^{-1} for high winds (12 m s^{-1}). Assuming $\Gamma = 0.2$, these are equivalent to average dissipation rates of 2×10^{-6} m^2 s^{-3} and 1×10^{-5} m^2 s^{-3}, which are one to two orders of magnitude lower than rates observed in the front or near field. However, wind typically acts over the entire plume, and the spatial area of active mixing may be large enough to make the net effect substantial.

Mixing of the plume by the wind relies primarily on shear in the surface Ekman layer. Ekman transport in the surface layer will be constant for a given wind stress, but the flow speed is inversely

proportional to the plume depth. A model of plume mixing by the wind was presented by Fong & Geyer (2001) and later modified by Lentz (2004) and Hetland (2005). The wind drives Ekman transport in the plume layer, which drives vertical shear and shear mixing. As described by Fong & Geyer (2001), the influence of wind on the far-field plume is modified by upwelling or downwelling winds, which tend to thin or thicken the plume, respectively, thus modifying the mixing response.

It is convenient to define a freshwater thickness, $h_f = \int_{-H}^{\eta} (S_0 - S)/S_0 \, dz$, which is the vertical integral of the salinity anomaly, $S_0 - S$, relative to the ambient water salinity, S_0. An upper limit to g' is defined as $g'_f = g \Delta\rho_f \rho_0^{-1}$, where $\Delta\rho_f$ is the density difference between purely freshwater and ambient water. By combining conservation of mass, $g' h_p = g'_f h_f$, the Ekman transport equation, $u_E h_p = \tau f^{-1}$, and the definition of the critical bulk Richardson number, $\mathrm{Ri}_c = g' h_p U_E^{-2}$, one can calculate the critical plume thickness for a given wind stress as

$$h_p = \frac{2\tau}{\rho_0 f} \sqrt{\frac{\mathrm{Ri}_c}{g'_f h_f}}. \tag{4}$$

The plume will mix to the critical depth, which depends on the wind stress and freshwater thickness, and then mixing will be suppressed. If the plume has already mixed to this point, or past it, no further mixing will occur. Thus, in this case, the wind supplies the kinetic energy for mixing, but it is modulated by rotation in a way that prevents the wind from continually accelerating the fluid. In a nonrotating case, a continuously applied wind would keep accelerating the fluid, and the plume would continually mix. Thus, rotation limits the amount of mixing that can occur for a given wind stress.

Wave breaking generates intense turbulence at the ocean surface, with observed dissipation rates reaching values of 10^{-3}–10^{-1} m^2 s^{-3} in typical wind waves (Agrawal et al. 1992, Gemmrich 2010, Thomson 2012). The wave height is the primary scale that determines the penetration depth of breaking wave–enhanced turbulence (Terray et al. 1996), suggesting that plumes may be strongly influenced by wave breaking when their thickness is of the same order as the wave height, although this has yet to be tested in the field. Using a numerical model, Gerbi et al. (2013) find that wave breaking has a substantial effect on the structure and dynamics of a river plume but find little impact of wave breaking on mixing, presumably because the plume they investigate is too thick to feel the effect of intensified surface turbulence at the density interface. Wave breaking is parameterized in their model as a surface source of turbulent kinetic energy that diffuses down into the water column, following Craig & Banner (1994).

3.1.3. Frontal mixing. Intense turbulence is often observed in plume fronts generated by energetic tidal plumes, with dissipation rates on the order of 10^{-4}–10^{-3} m^2 s^{-3} (Orton & Jay 2005, O'Donnell et al. 2008, Horner-Devine et al. 2013), which are of a similar magnitude to those observed in the near-field plume region. However, the contribution of the front to the mixing budget of the plume and the magnitude of this contribution relative to mixing in the near- or far-field plume regions are still uncertain. Current estimates of the frontal mixing contribution to the total mixing range from approximately 100% (Pritchard & Huntley 2006) to 20% (Orton & Jay 2005) and possibly much less (Cole 2014). Whereas turbulence is very high in the plume front, it decays exponentially behind the front (O'Donnell et al. 2008, Horner-Devine et al. 2013), resulting in a narrow band of active mixing. O'Donnell et al. (2008) estimate the size of the frontal mixing region based on laboratory grid turbulence experiments (Itsweire et al. 1993) as $L_I = 5\, u_{\mathrm{fr}}\, N^{-1}$, resulting in estimates ranging from 15 m in the Connecticut River plume to 60 m in the Columbia River plume. Here u_{fr} is the frontal propagation speed. The total area of frontal mixing is a function of L_I and the plume circumference, both of which may change as the plume front propagates offshore.

Kilcher & Nash (2010) show that the frontal Froude number $\mathrm{Fr} = u_{\mathrm{fr}}\,(g'h)^{-1/2}$ in the Columbia River plume is relatively constant in the tidal plume front during ebb tides, in large part because of increasing freshwater flux from the estuary. This suggests that mixing may be maintained as the frontal circumference increases, at least in a large tidal plume such as the Columbia River plume. As the ebb tide ends and the estuary discharge decreases, the front speed drops below the ambient internal wave speed, and it releases internal solitons, losing further energy to the wave field (Nash & Moum 2005; Jay et al. 2009, 2010).

3.1.4. Mixing in the bottom boundary layer. When a plume interacts with the seafloor, there may be convective adjustment owing to Ekman transport in the bottom boundary layer (see Section 4.6). Although it is widely accepted that this process influences the plume frontal position, it is not well understood how the associated mixing alters plume water masses. In shallow shelves with strong tides, bottom stress associated with the tidal flow may mix the plume from the bottom. This is more common in the type of broad, shallow seas that are found in northern Europe and are referred to as ROFIs (see Simpson 1997). In these regions, the interaction of the rotational, oscillatory bottom boundary layer with the plume's stratification results in counter-rotating tidal ellipses in the surface and bottom layers (Visser et al. 1994, Souza & Simpson 1996). This form of tidal straining can periodically increase and decrease the vertical stratification (De Boer et al. 2006, 2008), can cause the plume to periodically separate from the coast (De Boer et al. 2009), and may drive mixing (Fisher et al. 2002).

3.2. Integrated Plume Mixing: Quantifying and Comparing Mixing Within and Across Plumes

The net dilution of freshwater as it traverses through a plume is determined by the sum of the mixing processes and is thus essential in a complete description of plume mixing and transport. To understand how the different mixing processes described in Section 3.1 combine to produce the total dilution of the plume and to compare the relative contributions of each, one needs to develop a framework for comparison.

3.2.1. Mixing budget. Many studies investigate the role of mixing in the context of an energy balance (e.g., Winters et al. 1995, Wunsch & Ferrari 2004, MacCready et al. 2009). The most relevant to the present review is that by MacCready et al. (2009), who investigate mixing in the Columbia River plume using an energy balance for the estuary and plume regions. MacCready et al. show how three types of energy—kinetic energy associated with the flow field, barotropic energy associated with sea surface height displacements, and baroclinic energy associated with density differences—change in response to various forcing terms. The energy balances in the Columbia River estuary and plume show that pressure work dominates the balance in the estuary, whereas either winds or tides were most important for driving mixing in the plume, depending on the relative strength of the winds and the magnitude of the tides. Although mixing is observed to be weaker, more heterogeneous, and more episodic in the wind-driven plume than in the estuary, the net mixing is a significant component of the total energy budget in both. The energy balance approach is most effective when hydrodynamic model results are used that capture the full spatial and temporal variability of a system; it is virtually impossible to generate sufficient observational data to adequately evaluate the mixing budget as described by MacCready et al. (2009).

3.2.2. Comparison of plume mixing estimates. Although considerable work has been done to estimate mixing rates in different regions of the plume, we are still unable to quantify the relative

importance of each process or region in the net mixing in a plume. A notable exception is work by Pritchard & Huntley (2006), who compare wind, tidal, and frontal mixing within the River Teign plume. They argue that these three processes can explain all the mixing required to completely disperse the small, tidally pulsed plume. Pritchard & Huntley model mixing in this system based on in situ observations. Using a potential energy budget that is much simpler than that in MacCready et al. (2009), they estimate the magnitudes of net wind, tidal, and frontal mixing and compare them to the total potential energy supplied by the buoyant outflow. Their energy budget is based on

$$\phi = \frac{1}{\eta + H} \int_{-H}^{\eta} gz(\bar{\rho} - \rho)\, dz, \tag{5}$$

where $\bar{\rho}$ is the vertical mean density. The term ϕ represents the mechanical energy required to vertically homogenize the water column and is used as a metric to quantify stratification (e.g., Simpson et al. 1981, Burchard & Hofmeister 2008).

The River Teign forms a very small plume with $Q_f \sim 5\ \mathrm{m^3\ s^{-1}}$; its plume is mixed out entirely on each tide and forms anew on the following ebb. Pritchard & Huntley (2006) find that frontal mixing dominates in this plume and is capable of mixing 100% of the buoyancy input on each tide. Wind mixing is only comparable to frontal mixing with winds between 15 and 20 $\mathrm{m\ s^{-1}}$, and tidal mixing is always negligible. This result is in sharp contrast to the results from the Columbia River plume (MacCready et al. 2009), suggesting that the relative contributions of each mixing process depend on the magnitude of the river discharge and plume.

The normalization presented by Pritchard & Huntley (2006) provides a framework for comparing the relative importance of different mixing mechanisms in the dilution of a plume. It considers the rate of energy converted to mixing due to a specific process relative to the total energy required to mix the freshwater discharge completely into the ambient ocean. We express this ratio here as the ratio of the turbulent buoyancy flux B for an individual mixing process to the available potential energy from the estuary:

$$M = 2\frac{BA}{g_f' Q}\gamma T^*, \tag{6}$$

where $\gamma = g_M'(g_f' - g_M')^{-1}$, and A is the horizontal area over which the buoyancy flux acts. The mixing normalization M differs from that of Pritchard & Huntley (2006) in two ways. First, we consider the amount of energy required to mix the discharge from its initial g_0' to a final g_M', instead of complete mixing over the entire water depth. Second, we introduce a nondimensional time variable T^*, which represents the fraction of time for which the process is active. For example, T^* is between 0.3 and 0.5 for a process that occurs only on the ebb tide. In theory, individual M terms representing the various components of a single plume realization should sum approximately to 1.

Measurements of ϵ or B from observations in various regions (e.g., Luketina & Imberger 1987, Houghton et al. 2004, MacDonald & Geyer 2004, Orton & Jay 2005, MacDonald et al. 2007, McCabe et al. 2008, O'Donnell et al. 2008, Kilcher et al. 2012, Horner-Devine et al. 2013) could be used to estimate M, but these estimates are typically point measurements, which must be assumed representative of processes over some unknown volume and time fraction. Approximations of the spatial and temporal extent of mixing can be made, in some cases more reliably than others, but in any case, they generally inject significant uncertainty into estimates of M from available field data.

A comparison of values of M estimated based on plume turbulence measurements summarized in Section 3.1 illustrates the challenges in constructing a meaningful mixing budget. Near-field

M values based on observations from the Columbia and Merrimack Rivers (e.g., MacDonald et al. 2007, Kilcher et al. 2012) appear reasonable and suggest that near-field mixing might be responsible for 10–30% of the total required mixing. However, estimates based on observations from the far-field regions of the Delaware Bay outflow and Hudson River (Houghton et al. 2004, 2009); frontal regions in the Columbia River (Orton & Jay 2005), Merrimack River (Horner-Devine et al. 2013), and Connecticut River (O'Donnell et al. 2008); and the mid-field plume region of the Columbia River (McCabe et al. 2008) appear far less robust, with values ranging from less than 0.2% to nearly 400%. Clearly, these observational estimates are significantly impacted by errors in estimating the volumetric extent of mixing and variability of mixing across plume regions. This highlights an important gap in our current understanding of plume dynamics, for which most studies to date are process oriented and focused on point measurements, which may or may not be representative of the entire plume over larger spatial and temporal scales.

The range of estimates above also highlights the difficulty in using temporally and spatially isolated measurements from different regions to draw broad conclusions about plume mixing. As conditions may vary from ebb to ebb, enhanced mixing in one region might decrease the energy available to mix in a subsequent region, thus altering the chain of *M* values leading to complete dilution. This highlights the fact that many different pathways to dilution may exist for a single system, depending on a variety of external forcing mechanisms. Hetland (2005) describes a plume as a series of connected regions, with each region setting the water properties that enter the next region. Although this mixing sequence has been well characterized using numerical models, these models necessarily involve parameterizations of the mixing processes. It is a tremendous observational challenge to resolve the mixing processes across the temporal and spatial scales of the plume necessary to accurately compare interconnected mixing processes acting in different regions of the plume. For example, using multiyear ferry-based measurements of the Fraser River plume, Halverson & Palowicz (2008) show that increased river discharge decreases the salinity of the water exiting the near field, thus quantifying the net mixing across the near-field plume under different forcing. Recent in situ measurements of the Columbia and Merrimack River plumes using multiple concurrent platforms may bring us closer to the goal of actively comparing interconnected mixing processes occurring in different regions of a plume. Also, recent advances in remote sensing may offer solutions to estimating mixing across the entire plume synoptically (Chickadel et al. 2011).

4. TRANSPORT

4.1. Plume Transport

Transport of river water away from the mouth is driven primarily by the plume's buoyancy, wind stress, and ambient coastal currents and is strongly mediated by Earth's rotation. Mixing processes near the river mouth or in the core of the near-field plume play an important role in plume transport because baroclinic pressure gradients, proportional to internal density gradients, drive plume transport. In the absence of significant external forcing, transport away from the river mouth may be dominated by the retention of river water in a persistent eddy feature referred to as the bulge. In this section, we describe the dominant parameters that modify the alongshore transport. Most alongshore transport occurs in the coastal current region of the plume, which is typically in geostrophic balance. However, winds, tides, and bottom slope will influence the structure and transport in the coastal current; this is described in order to present a full picture of the transport processes.

4.2. Control Volume Approach

Nof & Pichevin (2001) provide a theoretical framework for understanding the alongshore transport in a simplified river inflow. Their approach is based on the layer-averaged alongshore momentum equation, integrated over a control volume that bounds the river mouth region. Equation 7 is a generalized expression for the control volume–integrated alongshore momentum for a river entering at angle θ_i:

$$\underbrace{-\iint_A \frac{\partial}{\partial t}(uh)dxdy}_{M_t} + \underbrace{f\iint_A (vh)dxdy}_{M_C} + \underbrace{\frac{UQ}{2}\cos_i\left(2+\frac{1}{\mathrm{Fr}_i^2}\right)}_{M_i} + F_e = \underbrace{\oint_c \left(u^2h + \frac{g'h^2}{2}\right)dy}_{M_{cc}}. \quad (7)$$

M_t and M_C are the momentum contributions due to the unsteadiness of the plume and Coriolis force resulting from the net cross-shore velocity in the control volume, respectively. M_i is the inflow contribution of the alongshore momentum as well as the alongshore component of the baroclinic pressure force acting on the control volume at the inflow. This term is zero if the river inflow is perpendicular to the coast, $\theta_i = 90°$, and provides a contribution in the positive x direction if $\theta_i < 90°$. Fr_i is the inflow Froude number, based on the average inflow velocity, depth, and density anomaly. F_e represents the external forces acting on the plume, including winds, bottom drag, and the force imparted by ambient currents. M_{cc} is the momentum flux out of the control volume in the coastal current plus the baroclinic pressure force back on the control volume. Because it is positive definite, this term provides a force on the control volume in the negative x direction. It is important to note that Equation 7 is a layer model and does not explicitly include mixing processes. This is a reasonable approximation in systems in which winds and tidal mixing are low and much of the plume mixing occurs in the estuary and the near-field plume.

Pichevin & Nof (1997) consider the simplified case in which the inflow is perpendicular to the coast ($M_i = 0$), the flow is steady ($M_t = 0$), there is no net across-shore flow ($M_C = 0$), and there are no external forces ($F_e = 0$). In this case, no force exists to balance the flux of momentum into the coastal current M_{cc}, resulting in what they refer to as the momentum imbalance paradox. Because this is not possible, one of the neglected terms in Equation 7 must be nonzero.

4.3. The Bulge and the Reduction of Alongshore Flow

Nof & Pichevin (2001) conclude that the momentum equation can be satisfied if an unsteady growing recirculation region, referred to as the bulge, exists. The bulge, which is shown in **Figure 2**, is a persistent feature in most simplified numerical models (e.g., Oey & Mellor 1993, Kourafalou et al. 1996, Garvine 2001, Fong & Geyer 2002) and laboratory experiments (Avicola & Huq 2003a,b; Horner-Devine et al. 2006) simulating river plumes, when there is no ambient current and the wind stress is low or moderate. Bulge formation requires that the estuary width is narrow relative to the Rossby deformation radius [i.e., the Kelvin number $K = Wf(g'h)^{-1}$ is less than 1] (Garvine 1995, Huq 2009). When present, the bulge is a subtidal feature that grows continuously in time, accumulating between 25% and 75% of the river's freshwater discharge and causing a corresponding reduction in the transport of freshwater away from the river mouth region in the coastal current (Fong & Geyer 2002, Horner-Devine et al. 2006). The mechanism leading to retention in the bulge is associated with splitting of the buoyant current as it impinges on the coast at a stagnation point downstream of the river mouth. Based on the momentum balance presented by Whitehead (1985), the fraction that returns to the bulge rather than flowing into the coastal current depends on the incidence angle of the impinging bulge current (Avicola & Huq 2003a, Horner-Devine et al. 2006). Recently, a well-defined bulge circulation and

corresponding reduction in alongshore freshwater transport have been observed in large-scale field sampling efforts (e.g., Chant et al. 2008, Horner-Devine 2009). The unsteadiness of the bulge flow is documented in satellite observations (Horner-Devine et al. 2008), and its impacts on the coastal ecosystem have been observed (Chant et al. 2008, Kudela et al. 2010).

The bulge flow consists primarily of a large eddy rotating anticyclonically in which the momentum is in gradient-wind balance (Yankovsky & Chapman 1997; Nof & Pichevin 2001; Horner-Devine et al. 2006, 2009),

$$\frac{u_\theta^2}{r} + f u_\theta = g' \frac{\partial b}{\partial r}. \tag{8}$$

This balance is typically expressed in a cylindrical coordinate system in which u_θ is the azimuthal velocity and r is a radial coordinate with its origin at the center of the bulge. There is an initial setup period, during which the unsteady acceleration term $\partial u_r/\partial t$ is also important in the momentum balance. After this 1–2-day period, the bulge is in gradient-wind balance, despite the fact that it is continually expanding (Horner-Devine 2009). Nof & Pichevin (2001) assume $M_t \simeq 0$ and model the offshore expansion as a constant net cross-shore migration speed C_y, and the resulting alongshore momentum balance is between M_C and M_{cc}. If the bulge is in gradient-wind balance, this results in predictions for the central depth H_b, radius R_b, and migration speed C_y for the bulge (see Nof & Pichevin 2001). In their formulation, the alongshore transport in the coastal current is given by

$$\frac{Q_{cc}}{Q} = \frac{1}{1+2\alpha}, \tag{9}$$

where $\alpha = -2u_\theta/fr$ is the nondimensional bulge vorticity. When the potential vorticity is zero, corresponding to a relatively intense eddy with $\alpha = 1$, Equation 9 predicts that 33% of the river discharge will be transported away from the river mouth in the coastal current, and the remaining 67% will accumulate in the bulge. When the eddy is weaker ($\alpha \ll 1$), the coastal current transport is predicted to increase (**Figure 3**). Few field data exist to test Equation 9, but estimates from both the Columbia River (Horner-Devine 2009) and Hudson River (Chant et al. 2008) plumes suggest that it provides a reasonable prediction (**Figure 3**).

The drawback of Equation 9 is that it cannot provide an a priori estimate of the alongshore transport because it depends on the observed bulge vorticity α. Efforts to predict $Q_{cc}Q^{-1}$ a priori do so based on the inflow Rossby number $\mathrm{Ro}_i = U f^{-1} W^{-1}$ (Fong & Geyer 2002, Horner-Devine et al. 2006), which can be interpreted as the inflow vorticity. Here, U and W are the inflow velocity and width, respectively. $Q_{cc}Q^{-1}$ is less sensitive to Ro_i compared with the prediction for α (**Figure 3**). This may be related to the amount of mixing occurring in the near-field plume, which will determine the degree of modification of vorticity between the inflow and the bulge. A good understanding of how inflow conditions set α may provide the information necessary to generate an a priori prediction of alongshore plume transport for this simplified case.

4.4. The Role of Wind

In addition to mixing via Ekman shear (Section 3.1.2), wind may also translate a plume and enhance or limit transport. Wind is often the dominant driver of transport in a plume. In the case of a thin plume that is not in contact with the seafloor, this transport is straightforward and should correspond to $F_e \sim M_{cc}$. In general, a downwelling wind will enhance alongshore transport, whereas an upwelling wind will diminish it (Fong & Geyer 2001). An upwelling wind is an alongshore wind in the opposite direction to the coastal current that creates a divergent, offshore flow due to Ekman transport; a downwelling wind blows in the same direction as the coastal current

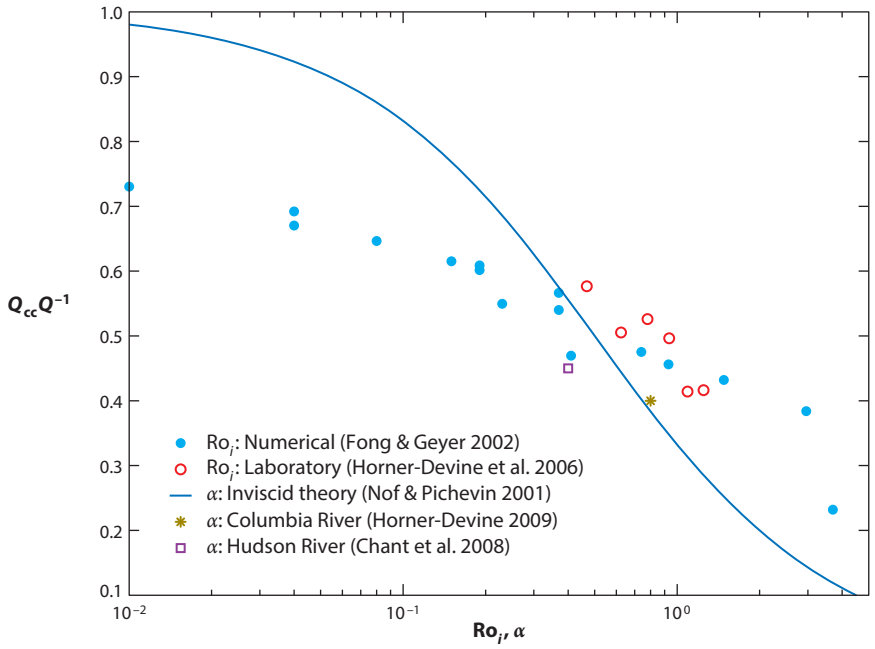

Figure 3

Comparison of theoretical predictions for the coastal current transport from **Equation 9** (Nof & Pichevin 2001) with numerical (Fong & Geyer 2002), experimental (Horner-Devine et al. 2006), and field observational (Chant et al. 2008, Horner-Devine 2009) estimates. Note that the abscissa is Ro for the laboratory and model data and α for the theory and field data. These correspond to estimates of the normalized vorticity at the inflow and in the bulge, respectively.

and creates a convergent, onshore flow. However, for a plume in which the pycnocline intersects a significant stretch of the seafloor, wind forcing is more complicated. For an unstratified shelf, the convergence or divergence of the Ekman transport at the coast will cause a setup or setdown of the sea level, which in turn will drive geostrophic alongshore currents in the same direction as the alongshore wind stress (e.g., Csanady 1977). Buoyancy-driven coastal currents will respond to the wind in the same way, with two notable modifications. First, the buoyancy-driven flow will be superimposed on the wind-driven currents, such that an upcoast wind will only drive upcoast currents if it can overpower the buoyancy-driven flow (Zhang & Hetland 2012). Second, the cross-shore density structure must evolve in response to the wind stress such that it is also in geostrophic balance with the wind-driven currents (Whitney & Garvine 2005, Zhang 2013).

4.5. Modification of Transport by Other Processes

Although the bulge flow described in Section 4.3 provides a useful baseline for understanding plume transport and presents a good target for analytical modeling, it is applicable only a fraction of the time in real plumes due to coastline geometry, ambient currents, tides, and winds that often dominate plume transport (e.g., Kudela et al. 2010).

When the inflow angle θ_i is reduced below 90°, the inflow contributes momentum in the alongshore direction that can act to balance the flux of momentum into the coastal current ($M_i \sim M_{cc}$). Thus, the offshore expansion and Coriolis term decrease, and more fluid is transported away

from the river mouth in the coastal current. Almost all the river discharge is carried downstream in the coastal current when θ_i is less than a critical angle between 40° and 60° (Garvine 2001, Avicola & Huq 2003b, Horner-Devine 2004). The propensity to generate a bulge is related to the degree of flow separation from the coast (Bormans & Garrett 1989) and is explained in terms of a separation ratio df/u, where d is the maximum offshore distance of the separated flow (Avicola & Huq 2003b).

Ambient along-coast currents can also significantly influence plume transport, augmenting transport if the current is in the same direction or decreasing transport if the current opposes the plume. Fong & Geyer (2002) show that the barotropic transport component augments the baroclinic transport that is present in the plume in the absence of an ambient current. Even a relatively small ambient current of 0.2 m s^{-1} is sufficient to increase the alongshore transport to match the river discharge.

Isobe (2005) reports that tidal currents stabilize the bulge and increase alongshore transport. His simulations suggest that after approximately 60 days, the coastal current transport is equal to the river discharge in small- to medium-sized discharges with tidal currents of 0.3 m s^{-1}.

4.6. Coastal Currents over Sloping Bathymetry

Near the source, there can be significant cross-shore currents and substantial mixing. Eventually, however, in the absence of prominent headlands or bays, the flow will evolve such that the currents are very nearly in geostrophic balance, oriented along shore, with density gradients primarily oriented offshore. The flow within the coastal current is in thermal wind balance such that the vertical shear is in balance with the horizontal density gradients. However, this balance does not set the transport of the coastal current, which is specified upstream by the value of Q_{cc}.

If a buoyancy-driven current interacts with the bottom, it will adjust such that the bottom flow is zero. Such balance is similar to the buoyancy arrest in the bottom boundary layer during upwelling conditions described by MacCready & Rhines (1993) but occurs through the entire water column. If the bottom currents are initially downcoast in the same sense as the surface buoyant flow, this will drive an offshore Ekman transport within the bottom boundary layer in which light coastal current water is pushed beneath heavier shelf water. The unstable water column mixes and reduces the integrated salinity at a particular depth due to the offshore flux of freshwater in the bottom boundary layer. The net effect of this process is to drive the plume front offshore, into deeper waters. Eventually the geostrophic transport within the plume front comes into balance with the thermal wind shear such that the flow at the bottom is approximately zero, thus halting further offshore migration of the plume front. This process is described in detail by Chapman & Lentz (1994) and Yankovsky & Chapman (1997) in a series of idealized numerical experiments. Curiously, these numerical experiments suggest that the cross-shore density gradients within the plume front remain roughly constant through the offshore migration process, such that the plume front retains its structure as it is pushed offshore. Observations (e.g., Kirincich & Hebert 2005) of buoyancy-driven flow over the continental shelf support the idea of buoyancy arrest; in fact, it is a very reasonable approximation to assume quiescent bottom currents for buoyancy-driven flows over the continental shelf at timescales of more than a few rotational periods.

Lentz & Helfrich (2002) and Avicola & Huq (2002) investigate the influence of a sloping bottom on the propagation of a plume. When the plume propagates along a vertical wall, the propagating nose is fed by currents along the wall, with a return flow back toward the source, relative to the translating nose. The nose propagation speed is given by $c_w = \sqrt{g' h_p} = (2Qg'f)^{1/4}$, where h_p is the maximum thickness of the plume, and Q is the net transport carried within the plume. If the plume propagates over a very gently sloping bottom, with slope α, with the propagation speed entirely determined by the bottom slope, the propagation speed reduces to $c_\alpha = \alpha g' f^{-1}$. For

intermediate cases, the propagation speed is

$$c_p = \frac{c_w}{1 + c_w/c_\alpha}. \tag{10}$$

This theory is able to explain the arrival time of pulses of freshwater from the Chesapeake River plume observed at Duck, North Carolina (Rennie et al. 1999).

5. DISCUSSION

5.1. Pathways of Dilution

Individual mixing and transport processes associated with freshwater discharge to the coastal ocean are the core components of any river plume system, and the isolation and investigation of these processes are the focus of most river plume studies to date. However, the integration of these individual processes creates the resulting plume structure and defines the pathway to dilution for terrestrially derived freshwater. As described in Section 2, freshwater dilution begins in the estuary, where a variety of mixing processes driven by tides and river discharge can serve to increase the discharge salinity before it reaches the coastline, and it continues offshore through a series of plume regions before its ultimate dissolution into the adjacent ocean waters. There are several resulting plume structures, depending on the relative importance of the various mixing and transport processes, resulting in a variety of dilution pathways. The nature of these pathways is critically important for identifying the overall fate and transport of the freshwater discharge, as well as any nutrients, pollutants, sediments, or other admixtures within the plume.

Owing to the addition of salt into the plume by mixing, the plume will become increasingly diluted as it evolves, characterized by an ever-decreasing density difference between the plume and ambient ocean waters. Thus, depending on the nature and strength of the mixing processes relative to the initial magnitude of the discharge, the dilution pathway may terminate at any stage, such that the far-field plume may be observed only for a subset of river discharges or may contain only a fraction of the total discharge.

In some cases, limited initial discharge or enhanced mixing may result in the dilution of the entire freshwater signal before the plume has time to pass through all the potential stages of its evolution (i.e., near field, mid-field/bulge, far field/coastal current). This is certainly the case for the River Teign plume (Pritchard & Huntley 2006) and other very small discharge plumes, but it is likely to be the case even for larger plumes, at least during specific times of the year. Other plumes, such as the Merrimack or Columbia River plumes (Hickey et al. 2010), may be dissolved within the mid-field region, depending on forcing conditions. Even plumes that lack a near-field region, such as the Delaware Bay plume, may be swept offshore and mixed away prior to the formation of a coherent coastal current, depending on wind conditions. Thus, a myriad of plume structures, and resulting pathways to dilution, can exist. **Figure 4** illustrates the possible dilution pathways that could exist, depending on various physical considerations at several critical points in the evolution of a plume. We note that in a single system, the dilution pathway and associated plume structure may shift as a function of river discharge, tidal range, winds, and so on, such that it is possible that a single system could at different times display many of the possible plume structures.

Most river discharges are associated with an estuary, where dilution begins in the laterally constrained lower reaches of the river channel. If freshwater discharge is high enough to maintain a supercritical value of Fr_1 at the river mouth through all phases of the tidal cycle, then no estuary exists, and all dilution processes are pushed into the unconfined coastal ocean. In very limited cases, with sufficiently small discharges, complete dilution could occur within the limits of the estuary,

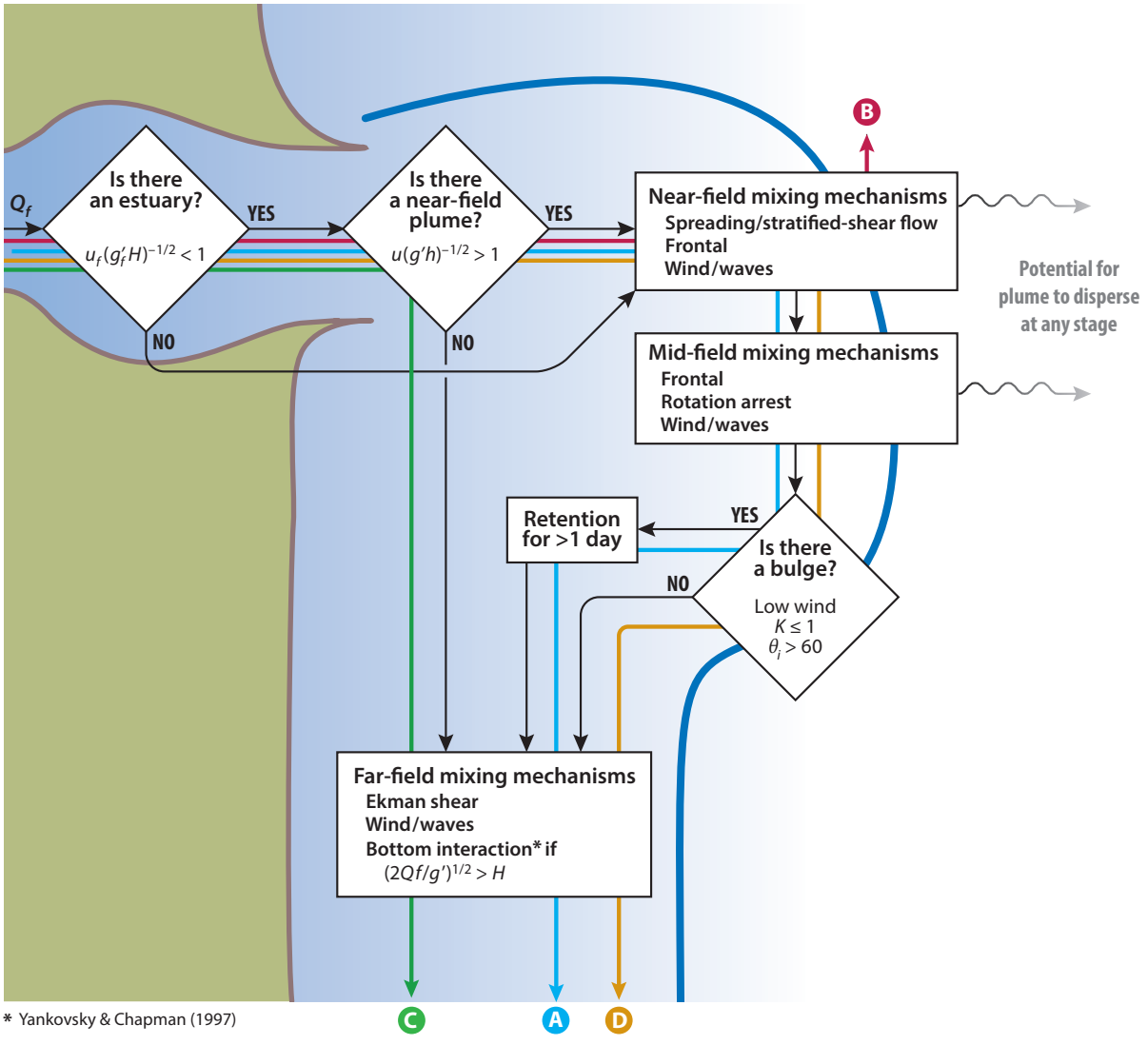

Figure 4

A schematic representation of mixing pathways in river plumes based on the presence or absence of different plume regions. Pathways A–D correspond to plumes A–D in **Figure 5**.

such that no plume is formed (see Geyer & MacCready 2014 for a detailed review of estuarine processes). The vast majority of discharge conditions are characterized by both an estuary and a plume.

At its simplest, the plume structure can be reduced to two defining aspects: (*a*) Does a supercritical near-field region exist, and (*b*) does a recirculating bulge exist? A near-field region exists if conditions at the mouth are supercritical with respect to an internal Froude number. If this condition is not met, then the plume will form a far-field plume or coastal current upon discharging from the estuary, with the dynamics of the forming plume strongly influenced by rotation.

If the supercritical condition is met, then a near-field region will be present until the outflow conditions are reduced to subcritical with respect to the internal Froude number at some distance (typically on the order of kilometers) from the river mouth. Beyond the near-field region lies a transition region, or mid-field plume, where the processes active in the near field transition to the geostrophic dynamics active in the far field. Ultimately, far enough downstream, the plume will become geostrophic, entering the final stage of plume dilution. All these regions may be influenced by winds, waves, background currents, and tidal currents. The relative importance of wind is typically considered to be weakest in the near field, where the inertia of the river discharge is dominant.

5.2. A Menagerie of Plumes

The variety of dilution pathways identified in **Figure 4** emphasizes that river plumes are multiscale flow structures comprising a number of distinct processes and regions. Plume dynamics are determined by stratified mixing processes operating at scales of 10^{-2}–10 m, large-scale transport processes at scales of 10^3–10^5 m, and a host of other processes that span the range between these scales. In an individual river plume, the processes that are most important are determined by the scale, geometry, and forcing of the plume. **Figure 5** shows a menagerie of plume morphologies, which represent most river plumes observed in the field. The imprint of some of these observed plume types is shown by the color-coded pathways in **Figure 4**. These plume types represent characteristic morphologies based largely on the geometry of the coast and the magnitude of the discharge. However, external forcing, such as wind in particular, will often alter the morphology of the plume such that the shape of the plume and the dilution pathways may be very different under different forcing conditions.

Prototypical plumes (plume A), comprising all dynamical regions, have a relatively high discharge and narrow mouth, and their dynamics are strongly modified by Earth's rotation. These plumes have the morphology observed in laboratory and numerical model experiments for a simplified coastal inflow. Examples exhibiting this morphology are the Columbia River plume (Hickey et al. 2010, 1998), the Merrimack River plume (MacDonald et al. 2007), the Niagara River plume (Masse & Murthy 1992, Horner-Devine et al. 2008), and the Hudson River plume (Chant et al. 2008). Important dynamical constraints in this type of plume include the internal Froude number, Fr_1, which sets the scale and intensity of the near field, and the Rossby number, which sets the scale for the downstream transition to a coastal current (Yankovsky & Chapman 1997) and the alongshore transport (Fong & Geyer 2002, Horner-Devine et al. 2006).

Nonrotational plumes (plume B), which have no mid-field or geostrophic coastal current, feel little effect of Earth's rotation, either because they are too small, as in the case of the River Teign plume (Pritchard & Huntley 2006), or because the river mouth is close to the equator, as in the case of the Amazon River plume (Lentz & Limeburner 1995). Their behavior is primarily characterized by an internal Froude number, Fr_1, resulting in various outflow conditions (Kashiwamura & Yoshida 1978), and can often be considered analogous to an engineering jet (e.g., Jirka et al. 1981, Atkinson 1993, Chen & MacDonald 2006, Jones et al. 2007). Many plumes in laboratory studies (e.g., Yuan & Horner-Devine 2013) are nonrotational and thus fall into this category.

Wide estuary plumes (plume C), which have no near field, a weak mid-field, and no bulge, have a sufficiently wide mouth that the freshwater separates from one side due to Earth's rotation inside the estuary. These plumes are similar to a geostrophic coastal current that adjusts as it rounds the corner into the coastal ocean, and as such comprise primarily far-field plumes. Classic examples include the Chesapeake Bay plume (e.g., Valle Levinson et al. 1998, Johnson et al. 2001, Dzwonkowski & Yan 2005) and the Delaware Bay plume (e.g., Whitney & Garvine 2006,

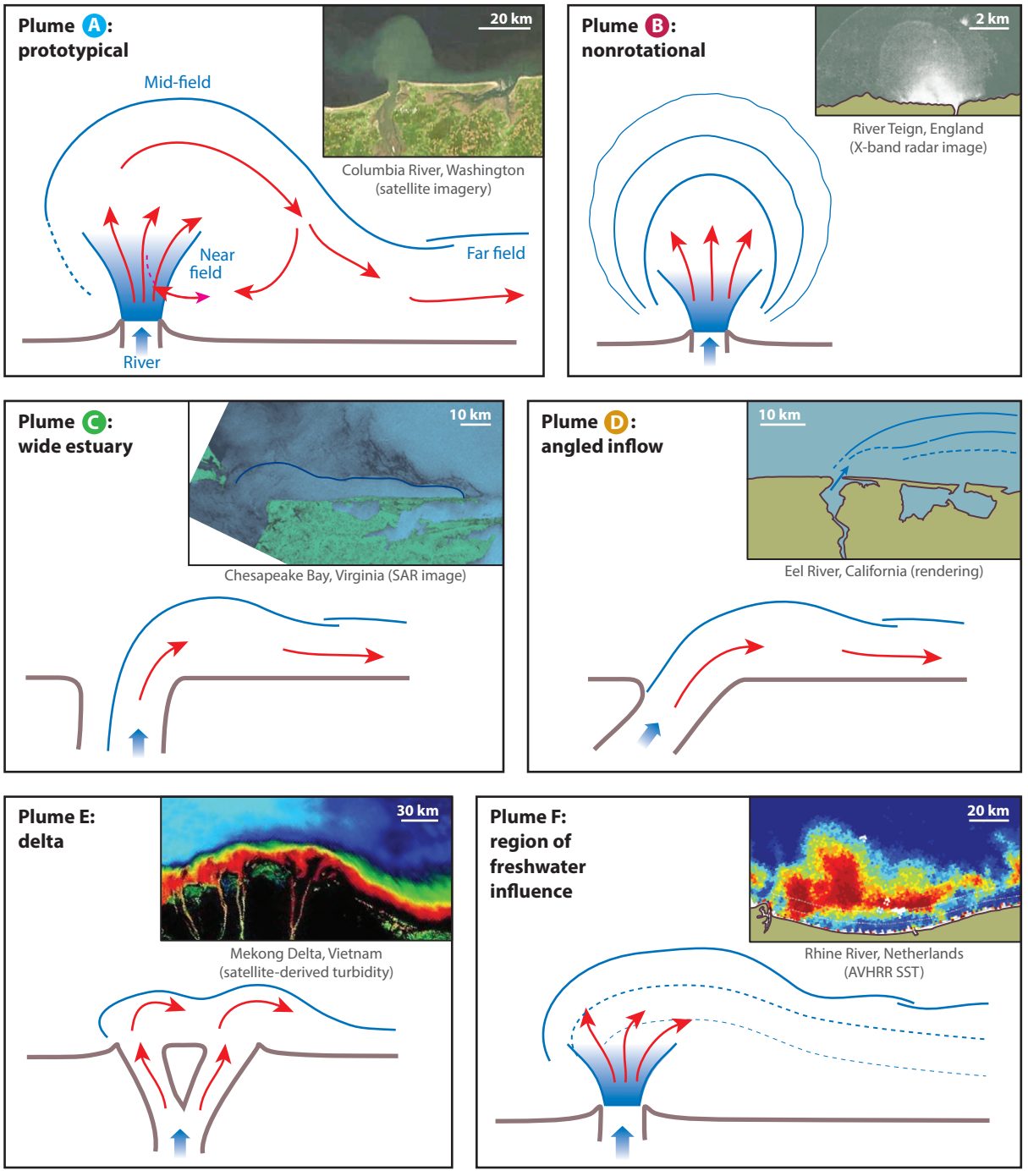

Figure 5

River plume morphologies: prototypical (plume A), nonrotational (plume B), wide estuary (plume C), angled inflow (plume D), delta plume (plume E), and region of freshwater influence (plume F). Inset images show examples of each plume type: (plume A) the Columbia River (SeaWiFS), (plume B) River Teign (Pritchard & Huntley 2006), (plume C) Chesapeake Bay (Donato & Marmorino 2002), (plume D) Eel River (Geyer et al. 2000), (plume E) Mekong River (Wisdom Project), and (plume F) Rhine River (De Boer et al. 2009).

Tilburg et al. 2007) outflows. In these plumes, rotation is of primary importance, and they can be characterized by the Ekman and Rossby numbers.

In angled inflow plumes (plume D), which typically have no bulge, the inflow is at a small angle to the coast, so it has a significant component of alongshore momentum initially. An example is the Eel River plume along the northern California coast (Geyer et al. 2000). This plume orientation can significantly affect plume transport, depending, in particular, on whether the inflow is aligned with or opposed to the direction of the coastal current. Depending on its size, this type of plume may be characterized by the internal Froude number or the rotational influences defined by the Ekman and Rossby numbers.

Delta plumes (plume E), which have mutually interacting regions, enter the ocean through a delta system, delivering freshwater via a number of river channels. Plumes formed by each of the channel outlets will interact with each other, depending on the spacing of the channels (Yuan et al. 2011). This formation is characteristic of many of the world's largest river systems (Wiseman & Garvine 1995), including the Mississippi (e.g., Wright & Coleman 1971), the Changjiang (Yangtze) (Beardsley et al. 1985), the Nile, and the Mekong Deltas. In this case, plume characterization is highly dependent on the overall size of the plume and also the nature and spacing of the individual distributaries.

In ROFIs (plume F), which have a strong interaction with the bottom, bottom friction is important and controls the cross-shore scale of the plume. Shallow marginal seas contribute to this type of plume being more prevalent along European coasts, with the Rhine (Simpson et al. 1993) and Liverpool Bay (Verspecht et al. 2009) as classic examples. The critical balance in these plumes exists between the destratifying effects of mixing due to bottom friction and the stratifying effects of sheared flow in the presence of lateral density gradients, characterized by the Simpson number,

$$\mathrm{Si} = \frac{\frac{g}{\rho_0}\frac{\partial \rho}{\partial x} H}{c_D U^2}. \tag{11}$$

5.3. Future Research Needs

Research on river plumes over the past several decades has resulted in the development of a framework for understanding the transformation of river discharge and its dissolution into the ambient ocean, including an idealized view of the plume structure and a detailed understanding of many mechanisms responsible for plume mixing. Modern numerical models have shown significant skill in predicting plume water properties, positions, and circulation patterns (MacDonald et al. 2007, Chant et al. 2008, Liu et al. 2009, Hetland & DiMarco 2012). However, significant gaps still exist in our understanding, including a mechanistic understanding of the role of winds and waves on plumes, the evolution of frontal mixing as plumes evolve, and the ultimate fate of river plumes as they merge into and alter ambient shelf and ocean waters. Perhaps more importantly, our understanding of plume mixing mechanisms focuses on specific locations within a plume. The significant spatial and temporal variability in plume structure and mixing processes precludes meaningful comparisons of these mixing estimates between plumes and even within the same plume system. Furthermore, no coherent scaling framework exists that sufficiently explains the relationships between plume forcing and mixing in various plume regions and that would enable intercomparisons among plume regions, among different forcing conditions for the same plume, and among different plume systems. Finally, no good methodology exists for making synoptic measurements of plume mixing. Thus, although significant advances have been made in understanding a few specific plume types and mixing process, we still lack a general framework in which to compare and contrast

all plume types and predict the dominant mixing mechanisms and circulation patterns within a plume.

DISCLOSURE STATEMENT

The authors are not aware of any biases that might be perceived as affecting the objectivity of this review.

ACKNOWLEDGMENTS

The authors would like to acknowledge support from National Science Foundation grants OCE-0550096, OCE-0850948, OCE-1233068, and OCE-0648655. A.R.H.-D. would also like to acknowledge support from the Allan and Inger Osberg Professorship.

LITERATURE CITED

Agrawal Y, Terray EA, Donelan MA, Hwang PA, Williams AJ III, et al. 1992. Enhanced dissipation of kinetic energy beneath surface waves. *Nature* 359:219–20

Armi L, Farmer DM. 1986. Maximal two-layer exchange through a contraction with barotropic net flow. *J. Fluid Mech.* 164:27–51

Atkinson JF. 1993. Detachment of buoyant surface jets discharged on a slope. *J. Hydraul. Eng.* 119:878–94

Avicola G, Huq P. 2002. Scaling analysis for the interaction between a buoyant coastal current and the continental shelf: experiments and observations. *J. Phys. Oceanogr.* 32:3233–48

Avicola G, Huq P. 2003a. The characteristics of the recirculating bulge region in coastal buoyant outflows. *J. Mar. Res.* 61:435–63

Avicola G, Huq P. 2003b. The role of outflow geometry in the formation of the recirculating bulge region in coastal buoyant outflows. *J. Mar. Res.* 61:411–34

Beardsley RC, Limeburner R, Yu H, Cannon GA. 1985. Discharge of the Changjiang (Yangtze River) into the East China Sea. *Cont. Shelf Res.* 4:57–76

Bormans M, Garrett C. 1989. The effect of rotation on the surface inflow through the Strait of Gibraltar. *J. Phys. Oceanogr.* 19:1535–42

Burchard H, Hofmeister R. 2008. A dynamic equation for the potential energy anomaly for analysing mixing and stratification in estuaries and coastal seas. *Estuar. Coast. Shelf Sci.* 77:679–87

Chant RJ. 2011. Interactions between estuaries and coasts: river plumes—their formation transport and dispersal. In *Treatise on Estuarine and Coastal Science*, Vol. 2, ed. E Wolanski, D McLusky, pp. 213–35. Amsterdam: Elsevier

Chant RJ, Wilkin J, Zhang W, Choi B, Hunter E, et al. 2008. Dispersal of the Hudson River Plume in theNew York Bight: synthesis of observational and numerical studies during LaTTE. *Oceanography* 21:148–61

Chapman DC, Lentz SJ. 1994. Trapping of a coastal density front by the bottom boundary layer. *J. Phys. Oceanogr.* 24:1464–79

Chen F, MacDonald DG. 2006. Role of mixing in the structure and evolution of a buoyant discharge plume. *J. Geophys. Res.* 111:C11002

Chen F, MacDonald DG, Hetland RD. 2009. Lateral spreading of a near-field river plume: observations and numerical simulations. *J. Geophys. Res.* 114:C07013

Chickadel CC, Talke SA, Horner-Devine AR, Jessup AT. 2011. Infrared-based measurements of velocity, turbulent kinetic energy, and dissipation at the water surface in a tidal river. *Geosci. Remote Sens. Lett. IEEE* 8:849–53

Cochrane JD, Kelly FJ. 1986. Low-frequency circulation on the Texas-Louisiana continental shelf. *J. Geophys. Res.* 91:10645–59

Cole KL. 2014. *A numerical study of the mid-field river plume*. PhD Thesis, Texas A&M Univ., College Station

Craig PD, Banner ML. 1994. Modeling wave-enhanced turbulence in the ocean surface layer. *J. Phys. Oceanogr.* 24:2546–59

Csanady GT. 1977. The coastal jet conceptual model in the dynamics of shallow seas. In *The Sea*, ed. I Goldberg, N O'Brian, JH Steele, pp. 117–44. New York: Wiley

De Boer GJ, Pietrzak JD, Winterwerp JC. 2006. On the vertical structure of the Rhine region of freshwater influence. *Ocean Dyn.* 56:198–216

De Boer GJ, Pietrzak JD, Winterwerp JC. 2008. Using the potential energy anomaly equation to investigate tidal straining and advection of stratification in a region of freshwater influence. *Ocean Model.* 22:1–11

De Boer GJ, Pietrzak JD, Winterwerp JC. 2009. SST observations of upwelling induced by tidal straining in the Rhine ROFI. *Cont. Shelf Res.* 29:263–77

Donato TF, Marmorino GO. 2002. The surface morphology of a coastal gravity current. *Cont. Shelf Res.* 22:141–46

Dzwonkowski B, Yan X-H. 2005. Tracking of a Chesapeake Bay estuarine outflow plume with satellite-based ocean color data. *Cont. Shelf Res.* 25:1942–58

Farmer DM, Armi L. 1986. Maximal two-layer exchange over a sill and through the combination of a sill and contraction with barotropic flow. *J. Fluid Mech.* 164:53–76

Fisher NR, Simpson JH, Howarth MJ. 2002. Turbulent dissipation in the Rhine ROFI forced by tidal flow and wind stress. *J. Sea Res.* 8:249–58

Fong DA, Geyer WR. 2001. Response of a river plume during an upwelling favorable wind event. *J. Geophys. Res.* 106:1067–84

Fong DA, Geyer WR. 2002. The alongshore transport of freshwater in a surface-trapped river plume. *J. Phys. Oceanogr.* 32:957–72

Garvine RW. 1984. Radial spreading of buoyant, surface plumes in coastal waters. *J. Geophys. Res.* 89:1989–96

Garvine RW. 1987. Estuary plumes and fronts in shelf waters: a layer model. *J. Phys. Oceanogr.* 17:1877–96

Garvine RW. 1995. A dynamical system for classifying buoyant coastal discharges. *Cont. Shelf Res.* 15:1585–96

Garvine RW. 2001. The impact of model configuration in studies of buoyant coastal discharge. *J. Mar. Res.* 59:193–225

Gemmrich J. 2010. Strong turbulence in the wave crest region. *J. Phys. Oceanogr.* 40:583–95

Gerbi GP, Chant RJ, Wilkin JL. 2013. Breaking surface wave effects on river plume dynamics during upwelling-favorable winds. *J. Phys. Oceanogr.* 43:1959–80

Geyer WR, Hill P, Milligan T, Traykovski P. 2000. The structure of the Eel River plume during floods. *Cont. Shelf Res.* 20:2067–93

Geyer WR, Lavery AC, Scully ME, Trowbridge JH. 2010. Mixing by shear instability at high Reynolds number. *Geophys. Res. Lett.* 37:L22607

Geyer WR, MacCready P. 2014. The estuarine circulation. *Annu. Rev. Fluid Mech.* 46:175–97

Halverson MJ, Palowicz R. 2008. Estuarine forcing of a river plume by river flow and tides. *J. Geophys. Res.* 113:C09033

Hetland RD. 2005. Relating river plume structure to vertical mixing. *J. Phys. Oceanogr.* 35:1667–88

Hetland RD. 2010. The effects of mixing and spreading on density in near-field river plumes. *Dyn. Atmos. Oceans* 49:37–53

Hetland RD, DiMarco SF. 2012. Skill assessment of a hydrodynamic model of circulation over the Texas-Louisiana continental shelf. *Ocean Model.* 43–44:64–76

Hetland RD, Hsu T-J. 2013. Freshwater and sediment dispersal in large river plumes. In *Biogeochemical Dynamics at Large River-Coastal Interfaces: Linkages with Global Climate Change*, ed. TS Bianchi, MA Allison, W-J Cai, pp. 55–85. New York: Springer

Hetland RD, MacDonald DG. 2008. Spreading in the near-field Merrimack River plume. *Ocean Model.* 21:12–21

Hickey BM, Kudela RM, Nash JD, Bruland KW, Peterson WT, et al. 2010. River influences on shelf ecosystems: introduction and synthesis. *J. Geophys. Res.* 115:C00B17

Hickey BM, Pietrafesa LJ, Jay DA, Boicourt WC. 1998. The Columbia River plume study: subtidal variability in the velocity and salinity fields. *J. Geophys. Res.* 103:10339–68

Horner-Devine AR. 2004. *The dynamics of buoyant, rotational river plumes*. PhD Thesis, Stanford Univ., Stanford, CA
Horner-Devine AR. 2009. The bulge circulation in the Columbia River plume. *Cont. Shelf Res.* 29:234–51
Horner-Devine AR, Chickadel CC, MacDonald DG. 2013. Coherent structures and mixing at a river plume front. In *Coherent Flow Structures in Geophysical Flows at the Earth's Surface*, ed. J Venditti, J Best, M Church, R Hardy, pp. 359–69. New York: Wiley
Horner-Devine AR, Fong DA, Monismith SG. 2008. Evidence for the inherent unsteadiness of a river plume: satellite observations of the Niagara River discharge. *Limnol. Oceanogr.* 53:2731–37
Horner-Devine AR, Fong DA, Monismith SG, Maxworthy T. 2006. Laboratory experiments simulating a coastal river discharge. *J. Fluid Mech.* 555:203–32
Horner-Devine AR, Jay DA, Orton PM, Spahn EY. 2009. A conceptual model of the strongly tidal Columbia River plume. *J. Mar. Sys.* 78:460–75
Houghton RW, Chant RJ, Rice A, Tilburg C. 2009. Salt flux into coastal river plumes: dye studies in the Delaware and Hudson River outflows. *J. Mar. Res.* 67:731–56
Houghton RW, Tilburg CE, Garvine RW, Fong A. 2004. Delaware River plume response to a strong upwelling-favorable wind event. *Geophys. Res. Lett.* 31:L07302
Huq P. 2009. The role of Kelvin number on bulge formation from estuarine buoyant outflows. *Estuaries Coasts* 32:709–19
Imberger J, Ivey GN. 1991. On the nature of turbulence in a stratified fluid. Part II: Application to lakes. *J. Phys. Oceanogr.* 21:659–80
Isobe A. 2005. Ballooning of river-plume bulge and its stabilization by tidal currents. *J. Phys. Oceanogr.* 35:2337–51
Itsweire EC, Koseff JR, Briggs DA, Ferziger JH. 1993. Turbulence in stratified shear flows: implications for interpreting shear-induced mixing in the ocean. *J. Phys. Oceanogr.* 23:1508–22
Ivey GN, Imberger J. 1991. On the nature of turbulence in a stratified fluid. I: The energetics of mixing. *J. Phys. Oceanogr.* 21:650–58
Ivey GN, Winters KB, Koseff JR. 2008. Density stratification, turbulence, but how much mixing? *Annu. Rev. Fluid Mech.* 40:169–84
Jay DA, Pan J, Orton PM, Horner-Devine AR. 2009. Asymmetry of tidal plume fronts in an eastern boundary current regime. *J. Mar. Sys.* 78:442–59
Jay DA, Zaron ED, Pan J. 2010. Initial expansion of the Columbia River tidal plume: theory and remote sensing observations. *J. Geophys. Res.* 115:C00B15
Jirka GH, Adams EE, Stolzenbach KD. 1981. Buoyant surface jets. *J. Hydraul. Div. Proc. ASCE* 107(HY11):1467–87
Johnson DR, Weidemann A, Arnone R, Davis CO. 2001. Chesapeake Bay outflow plume and coastal upwelling events: physical and optical properties. *J. Geophys. Res.* 106:11613–22
Jones GR, Nash JD, Doneker RL, Jirka GH. 2007. Buoyant surface discharges into water bodies. I: Flow classification and prediction methodology. *J. Hydraul. Eng.* 133:1010–20
Kantha L, Phillips O, Azad R. 1977. On turbulent entrainment at a stable density interface. *J. Fluid Mech.* 79:753–68
Kashiwamura M, Yoshida S. 1978. Outflow dynamics at a river mouth. *Proc. 16th Coast. Eng. Conf.*, pp. 2925–44. Reston, VA: Am. Soc. Civil Eng.
Kilcher L, Nash JD. 2010. Structure and dynamics of the Columbia River tidal plume front. *J. Geophys. Res.* 115:C05S90
Kilcher L, Nash JD, Moum JN. 2012. The role of turbulence stress divergence in decelerating a river plume. *J. Geophys. Res.* 117:C05032
Kirincich AR, Hebert D. 2005. The structure of the coastal density front at the outflow of Long Island Sound during spring 2002. *Cont. Shelf Res.* 25:1097–114
Kourafalou VH, Oey L-Y, Want JD, Lee TN. 1996. The fate of river discharge on the continental shelf: 1. Modeling the river plume and the inner shelf coastal current. *J. Geophys. Res.* 101:3415–34
Kudela RM, Horner-Devine AR, Banas NS, Hickey BM, Peterson TD, et al. 2010. Multiple trophic levels fueled by recirculation in the Columbia River plume. *Geophys. Res. Lett.* 37:L18607

Lentz SJ. 2004. The response of buoyant coastal plumes to upwelling-favorable winds. *J. Phys. Oceanogr.* 34:2458–67

Lentz SJ, Helfrich KR. 2002. Buoyant gravity currents along a sloping bottom in a rotating fluid. *J. Fluid Mech.* 464:251–78

Lentz SJ, Limeburner R. 1995. The Amazon River plume during AMASSEDS: spatial characteristics and salinity variability. *J. Geophys. Res.* 100:2355–75

Liu Y, MacCready P, Hickey BM, Dever EP, Kosro PM, Banas NS. 2009. Evaluation of a coastal ocean circulation model for the Columbia River plume in summer 2004. *J. Geophys. Res.* 114:C00B04

Luketina DA, Imberger J. 1987. Characteristics of a surface buoyant jet. *J. Geophys. Res.* 92:5435–47

MacCready P, Banas NS, Hickey BM, Dever EP, Liu Y. 2009. A model study of tide- and wind-induced mixing in the Columbia River estuary and plume. *Cont. Shelf Res.* 29:278–91

MacCready P, Geyer WR. 2010. Advances in estuarine physics. *Annu. Rev. Mar. Sci.* 2:35–58

MacCready P, Rhines PB. 1993. Slippery bottom boundary layers on a slope. *J. Phys. Oceanogr.* 23:5–22

MacDonald DG, Carlson J, Goodman L. 2013. On the heterogeneity of stratified-shear turbulence: observations from a near-field river plume. *J. Geophys. Res.* 118:6223–37

MacDonald DG, Chen F. 2012. Enhancement of turbulence through lateral spreading in a stratified-shear flow: development and assessment of a conceptual model. *J. Geophys. Res.* 117:C05025

MacDonald DG, Geyer WR. 2004. Turbulent energy production and entrainment at a highly stratified estuarine front. *J. Geophys. Res.* 109:C05004

MacDonald DG, Geyer WR. 2005. Hydraulic control of a highly stratified estuarine front. *J. Phys. Oceanogr.* 35:374–87

MacDonald DG, Goodman L, Hetland RD. 2007. Turbulent dissipation in a near-field river plume: a comparison of control volume and microstructure observations with a numerical model. *J. Geophys. Res.* 112:C07026

Masse AK, Murthy CR. 1992. Analysis of the Niagara River plume dynamics. *J. Geophys. Res.* 97:2403–20

McCabe RM, Hickey BM, MacCready P. 2008. Observational estimates of entrainment and vertical salt flux in the interior of a spreading river plume. *J. Geophys. Res.* 113:C08027

McCabe RM, MacCready P, Hickey BM. 2009. Ebb tide dynamics and spreading of a large river plume. *J. Phys. Oceanogr.* 39:2839–56

Milliman JD, Farnsworth KL. 2011. *River Discharge to the Coastal Ocean: A Global Synthesis*. Cambridge, UK: Cambridge Univ. Press

Milliman JD, Meade RH. 1983. World-wide delivery of river sediment to the ocean. *J. Geol.* 91:1–21

Moum JN, Gregg MC, Lien RC, Carr ME. 1995. Comparison of turbulence kinetic energy dissipation rate estimates from two ocean microstructure profilers. *J. Atmos. Ocean. Technol.* 12:346–66

Murray SP. 1998. *An observational study of the Mississippi-Atchafalaya coastal plume, final report*. Rep., US Dep. Inter., Miner. Manag. Serv., Gulf of Mexico OCS Reg.

Nash JD, Kilcher LF, Moum JN. 2009. Structure and composition of a strongly stratified, tidally pulsed river plume. *J. Geophys. Res.* 114:C00B12

Nash JD, Moum JN. 2005. River plumes as a source of large-amplitude internal waves in the coastal ocean. *Nature* 437:400–3

Nof D, Pichevin T. 2001. The ballooning of outflows. *J. Phys. Oceanogr.* 31:3045–58

O'Donnell J. 2010. The dynamics of estuary plumes and fronts. In *Contemporary Issues in Estuarine Physics*, ed. A Valle Levinson, pp. 186–246. Cambridge, UK: Cambridge Univ. Press

O'Donnell J, Ackleson SG, Levine ER. 2008. On the spatial scales of a river plume. *J. Geophys. Res.* 113:C04017

Oey L-Y, Mellor GL. 1993. Subtidal variability of estuarine outflow, plume, and coastal current: a model study. *J. Phys. Oceanogr.* 23:164–71

Orton PM, Jay DA. 2005. Observations at the tidal plume front of a high-volume river outflow. *Geophys. Res. Lett.* 32:L11605

Pichevin T, Nof D. 1997. The momentum imbalance paradox. *Tellus A* 49:298–319

Pritchard M, Huntley DA. 2006. A simplified energy and mixing budget for a small river plume discharge. *J. Geophys. Res.* 111:C03019

Rennie SE, Largier JL, Lentz SJ. 1999. Observations of a pulsed buoyancy current downstream of Chesapeake Bay. *J. Geophys. Res.* 104:18227–40

Sherman F, Imberger J, Corcos G. 1978. Turbulence and mixing in stably stratified waters. *Annu. Rev. Fluid Mech.* 10:267–88

Simpson JH. 1997. Physical processes in the ROFI regime. *J. Mar. Syst.* 12:3–15

Simpson JH, Bos WG, Schirmer F, Souza AJ, Rippeth TP, et al. 1993. Periodic stratification in the Rhine ROFI in the North Sea. *Oceanol. Acta* 16:23–32

Simpson JH, Crisp DJ, Hearn C. 1981. The shelf-sea fronts: implications of their existence and behaviour. *Philos. Trans. R. Soc. Lond. A* 302:531–46

Smyth W, Moum JN. 2000. Length scales of turbulence in stably stratified mixing layers. *Phys. Fluids* 12:1327–42

Smyth W, Moum JN, Caldwell DR. 2001. The efficiency of mixing in turbulent patches: inferences from direct simulations and microstructure observations. *J. Phys. Oceanogr.* 31:1969–92

Souza AJ, Simpson JH. 1996. The modification of tidal ellipses by stratification in the Rhine ROFI. *Cont. Shelf Res.* 16:997–1007

Stacey MT, Rippeth TP, Nash JD. 2011. Turbulence and stratification in estuaries and coastal seas. In *Treatise on Estuarine and Coastal Science*, Vol. 2, ed. E Wolanski, D McLusky, pp. 9–35. Amsterdam: Elsevier

Tedford EW, Carpenter JR, Pawlowicz R, Pieters R, Lawrence GA. 2009. Observation and analysis of shear instability in the Fraser River estuary. *J. Geophys. Res.* 114:C11006

Terray EA, Donelan MA, Agrawal YC, Drennan WM, Kahma KK, et al. 1996. Estimates of kinetic energy dissipation under breaking waves. *J. Phys. Oceanogr.* 26:792–807

Thomson J. 2012. Wave breaking dissipation observed with SWIFT drifters. *J. Atmos. Oceanic Technol.* 29:1866–82

Thorpe SA. 1969. Experiments on the stability of stratified shear flows. *J. Radio Sci.* 4:1327–31

Thorpe SA. 1973. Experiments on instability and turbulence in a stratified shear flow. *J. Fluid Mech.* 61:731–51

Tilburg C, Houghton RW, Garvine RW. 2007. Mixing of a dye tracer in the Delaware plume: comparison of observations and simulations. *J. Geophys. Res.* 112:C12004

Trenberth KE, Smith L, Qian T, Dai A, Fasullo J. 2007. Estimates of the global water budget and its annual cycle using observational and model data. *J. Hydrometeorol.* 8:758–69

Trowbridge JH. 1992. A simple description of the deepening and structure of a stably stratified flow driven by a surface stress. *J. Geophys. Res.* 97:15529–43

Valle Levinson A, Li C, Royer TC, Atkinson LP. 1998. Flow patterns at the Chesapeake Bay entrance. *Cont. Shelf Res.* 18:1157–77

Verspecht F, Rippeth TP, Howarth MJ, Souza AJ, Simpson JH, Burchard H. 2009. Processes impacting on stratification in a region of freshwater influence: application to Liverpool Bay. *J. Geophys. Res.* 114:C11022

Visser AW, Souza AJ, Hessner K, Simpson JH. 1994. The effect of stratification on tidal current profiles in a region of freshwater influence. *Oceanol. Acta* 17:369–81

Whitehead JA. 1985. The deflection of a baroclinic jet by a wall in a rotating fluid. *J. Fluid Mech.* 157:79–93

Whitney MM, Garvine RW. 2005. Wind influence on a coastal buoyant outflow. *J. Geophys. Res.* 110:C03014

Whitney MM, Garvine RW. 2006. Simulating the Delaware Bay buoyant outflow: comparison with observations. *J. Phys. Oceanogr.* 36:3–21

Winters KB, Lombard PN, Riley JJ, D'Asaro EA. 1995. Available potential energy and mixing in density-stratified fluids. *J. Fluid Mech.* 289:115–28

Wiseman WJ Jr, Garvine RW. 1995. Plumes and coastal currents near large river mouths. *Estuaries* 18:509–17

Wright LD, Coleman JM. 1971. Effluent expansion and interfacial mixing in the presence of a salt wedge, Mississippi River delta. *J. Geophys. Res.* 76:8649–61

Wunsch C, Ferrari R. 2004. Vertical mixing, energy, and the general circulation of the oceans. *Annu. Rev. Fluid Mech.* 36:281–314

Yankovsky AE, Chapman DC. 1997. A simple theory for the fate of buoyant coastal discharges. *J. Phys. Oceanogr.* 27:1386–401

Yuan Y, Averner ME, Horner-Devine AR. 2011. A two-color optical method for determining layer thickness in two interacting buoyant plumes. *Exp. Fluids* 50:1235–45

Yuan Y, Horner-Devine AR. 2013. Laboratory investigation of the impact of lateral spreading on buoyancy flux in a river plume. *J. Phys. Oceanogr.* 43:2588–610

Zhang X, Hetland RD, Marta-Almeida M, DiMarco SF. 2012. A numerical investigation of the Mississippi and Atchafalaya freshwater transport, filling and flushing times on the Texas-Louisiana Shelf. *J. Geophys. Res.* 117:C11009

Zhang Z. 2013. *Wind- and buoyancy-modulated along-shore circulation over the Texas-Louisiana shelf*. PhD Thesis, Texas A&M Univ., College Station

Zhang Z, Hetland RD. 2012. A numerical study on convergence of alongshore flows over the Texas-Louisiana shelf. *J. Geophys. Res.* 117:C11010

Annual Review of
Fluid Mechanics

Volume 47, 2015

Contents

Indexes

Errata

An online log of corrections to *Annual Review of Fluid Mechanics* articles may be found at http://www.annualreviews.org/errata/fluid